Imaging Electronic Excitation of NO by Ultrafast Laser Tunneling Ionization

Tomoyuki Endo,[1] Akitaka Matsuda,[1] Mizuho Fushitani,[1] Tomokazu Yasuike,[2] Oleg I. Tolstikhin,[3]
Toru Morishita,[4] and Akiyoshi Hishikawa[1,*]

[1]*Department of Chemistry, Graduate School of Science, Nagoya University, Furo-cho, Chikusa, Nagoya, Aichi 464-8602, Japan*
[2]*The Open University of Japan, Mihama, Chiba 261-8586, Japan*
[3]*Moscow Institute of Physics and Technology, Dolgoprudny 141700, Russia*
[4]*Institute for Advanced Science, The University of Electro-Communications, 1-5-1 Chofu-ga-oka, Chofu, Tokyo 182-8585, Japan*
(Received 13 November 2015; published 20 April 2016)

Tunneling-ionization imaging of photoexcitation of NO has been demonstrated by using few-cycle near-infrared intense laser pulses (8 fs, 800 nm, 1.1×10^{14} W/cm^2). The ion image of N$^+$ fragment ions produced by dissociative ionization of NO in the ground state, NO $(X^2\Pi, 2\pi) \rightarrow$ NO$^+ + e^- \rightarrow$ N$^+ +$ O $+ e^-$, exhibits a characteristic momentum distribution peaked at 45° with respect to the laser polarization direction. On the other hand, a broad distribution centered at ~0° appears when the $A^2\Sigma^+$ $(3s\sigma)$ excited state is prepared as the initial state by deep-UV photoexcitation. The observed angular distributions are in good agreement with the corresponding theoretical tunneling ionization yields, showing that the fragment anisotropy reflects changes of the highest-occupied molecular orbital by photoexcitation.

Recent developments of ultrafast spectroscopy have realized real-time observation of molecular processes at femto- and attosecond time scales, enabling us to track ultrafast electron dynamics associated with nonadiabatic transitions in photochemical reactions [1,2] and attosecond dynamics of electron wave packets [3,4]. In addition to conventional pump-probe schemes, several new approaches have been proposed in the past decades for direct visualization of the highest-occupied molecular orbitals (HOMOs) or the spatial distribution profile of electrons, by using molecular-frame photoelectron angular distribution [5,6], $(e, 2e)$ electron scattering [7], and high-order harmonics generation [8–10].

Alternatively, electron distribution profiles can be obtained by utilizing tunneling ionization in intense laser fields. Since the tunneling ionization rate is determined by the shape of HOMO along the laser electric field [11,12], one can capture the electron distribution profiles at a long distance from the ion core by measuring the ionization yields against the laser polarization direction in the molecular frame. Such measurements can be performed by using spatially aligned or oriented molecules as demonstrated for N$_2$, O$_2$, CO$_2$ [13], and OCS [14], or by electron-ion coincidence measurements [15,16]. Instead, the anisotropy of the ionization rates can be obtained from spatial distributions of fragment ions produced by Coulomb explosion of randomly oriented molecules. For example, the difference between the HOMOs of N$_2$ and O$_2$ is clearly seen in fragment-ion momentum images [17].

These previous experiments were carried out on molecules in their ground states. The extension to electronically excited states is of significant importance for real-time visualization of electron dynamics in photochemical reactions. However, the applicability to excited molecules is not trivial because of a substantial decrease in the ionization potentials, which may introduce significant contributions from multiphoton processes. Here we discuss tunneling-ionization imaging of electron distribution profiles in excited molecules. We adopted nitric oxide (NO) as the target, which has a low-lying electronic state $(A^2\Sigma^+)$ in the deep UV (DUV) range from the ground state $(X^2\Pi)$ (Fig. 1). The electronic configuration is $1\sigma^2 2\sigma^2 3\sigma^2 4\sigma^2 5\sigma^2 1\pi^4 2\pi^1 3s\sigma^0$ in the ground state, while $1\sigma^2 2\sigma^2 3\sigma^2 4\sigma^2 5\sigma^2 1\pi^4 2\pi^0 3s\sigma^1$ is dominant in the excited state [18–20]. The effect of photoexcitation from 2π to $3s\sigma$ is studied by momentum imaging of N$^+$ fragment ions, produced by dissociative ionization (DI) of NO, NO $\rightarrow$ N$^+ +$ O $+ e^-$. The experimental results are compared with theoretical tunneling-ionization yields from the weak-field asymptotic theory (WFAT) [21,22] under adiabatic conditions.

The output of a Ti:sapphire laser amplifier system (800 nm, ~2 mJ/pulse, 40 fs, 1 kHz) was split into two beams. One was introduced to a hollow-fiber pulse compressor to obtain few-cycle intense near-infrared (NIR) laser pulses (8 fs) for laser tunneling ionization. The other was used to obtain UV pulses (315 nm) by an optical parametric amplifier, which are further mixed with the fundamental pulses in a BBO crystal to generate DUV pulses at 226 nm (0.6 μJ/pulse). The center wavelength of the DUV pulses was tuned to the NO A-X (0,0) transition [23] to pump NO molecules to the $A^2\Sigma^+$ state (see Fig. 1). The pump (DUV) and probe (NIR) pulses were coaxially introduced to the vacuum chamber with a time delay of 150 ps and focused by a concave mirror ($f = 75$ mm) to an NO molecular beam. Contributions from vibrationally
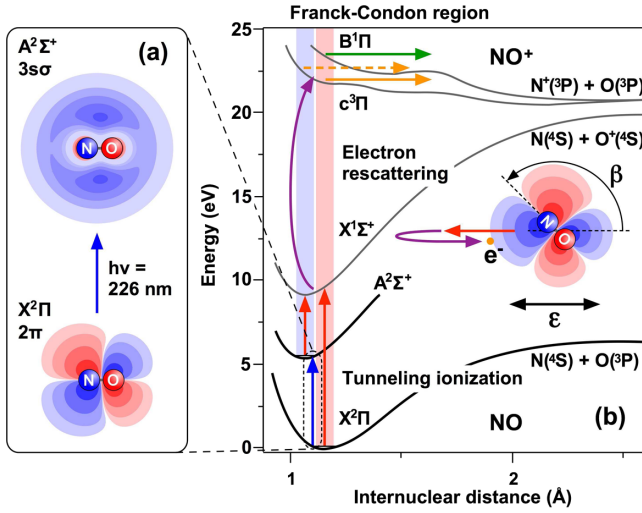
FIG. 1. (a) The highest-occupied molecular orbitals, 2π and $3s\sigma$, in the $X^2\Pi$ and $A^2\Sigma^+$ state. (b) Dissociative ionization of NO in intense laser fields by tunneling ionization and electron rescattering. Potential energy curves are adopted from Refs. [18–20]. The Franck-Condon region for the $X^2\Pi$ state, and that for the $A^2\Sigma^+$ state prepared by DUV excitation (226 nm), are shown with red and blue bars, respectively. The horizontal arrows indicate the energies of the $c^3\Pi$ state (orange) and the $B^1\Pi$ state (green) populated by the corresponding Franck-Condon transitions. The inset shows the definition of the molecular-axis angle β, where an arrow with ε represents the laser polarization direction.
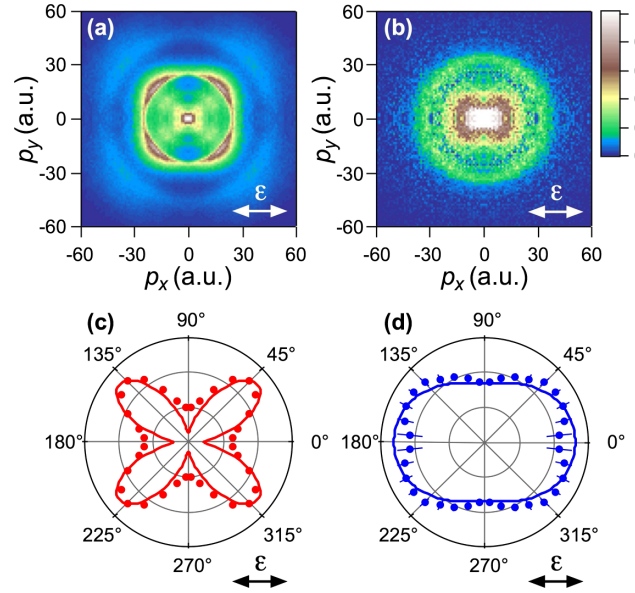

FIG. 2. Momentum images of the N^+ fragment ions produced by DI starting from (a) the $X^2\Pi$ state and (b) the $A^2\Sigma^+$ state in few-cycle intense laser fields (8 fs, 1.1×10^{14} W/cm^2). Symmetries with respect to the x and y axis are utilized to reduce the statistical uncertainty. The probe NIR laser polarization direction is denoted with ε. (c),(d) Polar plots of the fragment angular distributions obtained for the $X^2\Pi$ and $A^2\Sigma^+$ initial states, respectively. The distributions are evaluated on the $c^3\Pi$ dissociation pathway (see text). Solid lines are theoretical tunneling-ionization yields calculated by WFAT under the adiabatic approximation.

excited states are negligible in both the $X^2\Pi$ and $A^2\Sigma^+$ states under the present experimental conditions. The intensity of the probe pulse at the focal spot was estimated to be 1.1×10^{14} W/cm^2. The N^+ fragment ions produced by the dissociative ionization were guided by four electrodes to a position sensitive detector [24]. The three-dimensional momentum vector $\mathbf{p}_{N^+} = (p_x, p_y, p_z)$ was calculated from the position (x, y) on the position sensitive detector and the flight time (t) for each ion-detection event [25]. The total kinetic energy release (KER) was obtained as $E_{kin} = (m_N + m_O)/(2m_N m_O)|\mathbf{p}_{N^+}|^2$, with m_N and m_O being the mass of N^+ and O, respectively. Here the momentum of the counterpart O atom was assumed to be equal to $-\mathbf{p}_{N^+}$ by momentum conservation. Uncertainties in E_{kin} associated with electron recoil are estimated to be 2% and 4% at $E_{kin} = 1$ eV for the ground and excited states, respectively [26]. Since the amount of NO pumped to the $A^2\Sigma^+$ state is about 0.5% under the present experimental conditions, an optical chopper (0.5 kHz) was introduced to block the pump pulse in every other shot. The contributions from the DUV pulse alone were recorded separately.

The fragment momentum image of N^+ for the ground state ($X^2\Pi$) is shown in Fig. 2(a). The momentum distribution consists of two concentric features at $|\mathbf{p}| \sim 25$ and ~ 50 a.u., both of which are peaked at about 45° with respect to the laser polarization direction. The

corresponding features are observed in the total KER spectrum (A) at 0.65 and 2.2 eV (Fig. 3). These values are in good agreement with those observed for DI by single-photon absorption in vacuum UV [27], which are assigned to dissociation via the $c^3\Pi$ and $B^1\Pi$ states of NO$^+$, respectively [see Fig. 1(b)]. The agreement shows that DI in the present case proceeds from the Franck-Condon region of NO in the ground state. Along with the polarization ellipticity dependence in Fig. 4, this indicates that these repulsive states are excited by the rescattering electron [28,29], which occurs in a short time scale within an optical cycle of the laser field (2.7 fs). The maximum collision electron energy is $3.2U_p = 21$ eV at the field intensity of 1.1×10^{14} W/cm^2, where U_p is the ponderomotive potential. This is sufficiently larger than the excitation threshold energies, $E_{th} = 12.5$ and 13.5 eV, for the $c^3\Pi$ and $B^1\Pi$ states from the ground state of NO$^+$. Since the electronic excitation is considered almost isotropic [17], the fragment anisotropy reflects the tunneling ionization rates in the molecular frame, determined by 2π HOMO of the ground state of NO. It should be noted that the asymmetry of the molecular orbital associated with the difference between N and O cannot be accessed in the present experiments using randomly oriented molecules. Asymmetry-sensitive measurements on such samples can
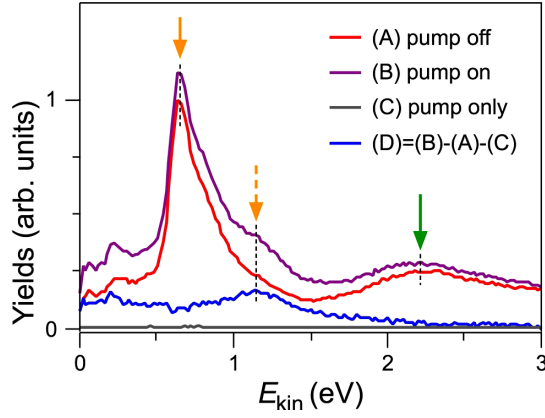
FIG. 3. The total KER spectra obtained with (A) pump off, (B) pump on, (C) pump only, and (D) the net signal, where spectra (A) and (D) correspond to the spectra of the dissociative ionization from the $X^2\Pi$ and $A^2\Sigma^+$ states, respectively. The arrows indicate peaks assigned to the $c^3\Pi$ and $B^1\Pi$ dissociation pathways [see Fig. 1(b)].

be performed, for example, by using carrier-envelope-phase-locked few-cycle pulses having asymmetric electric-field amplitudes.

The KER spectrum obtained with both the DUV pump and NIR probe pulses (B) is plotted in Fig. 3, together with that obtained with the DUV pulse alone (C). The net contribution from the excited NO in the $A^2\Sigma^+$ state (D) is obtained by $(D) = (B) - (A) - (C)$. The resultant spectrum exhibits a clear peak at $E_{kin} = 1.2$ eV with a broad hump on the lower energy side between 0 and ~0.6 eV. The broad hump, also seen in the KER distribution for the $X^2\Pi$ state, is attributed to the enhanced ionization at longer internuclear distances [30] as it increases drastically with a longer laser pulse (40 fs).
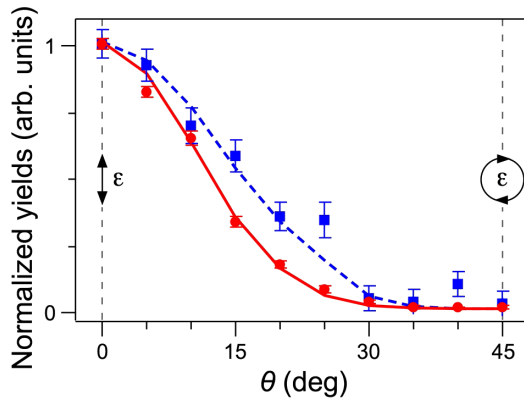

FIG. 4. Relative yields of N^+ fragment ions as a function of the angle θ of a quarter-wave plate with the $X^2\Pi$ (red circles) and $A^2\Sigma^+$ (blue squares) states of NO as the initial state. The solid line is a result of the least-squares fitting to the experimental data for the ground state, while the dashed line represents a theoretical prediction for the excited state (see text for details).

The peak observed at 1.2 eV is assigned to DI via the $c^3\Pi$ state of NO^+. The increase in KER as well as the broadening of the peak is attributed to the shift of the Franck-Condon window to the steeper part of the $c^3\Pi$ potential [see Fig. 1(b)], associated with the change in the equilibrium internuclear distance from $R_e(X^2\Pi) = 1.15$ Å to $R_e(A^2\Sigma^+) = 1.06$ Å [31]. Note that the $B^1\Pi$ component from the excited state is expected to appear at 3.6 eV, which is outside the detection range of the present experimental setup.

Figure 2(b) shows the net momentum image of N^+ produced from DI of the excited NO ($A^2\Sigma^+$) obtained after the background subtraction. The $c^3\Pi$ component at $|\boldsymbol{p}| \sim 32$ a.u. ($E_{kin} \sim 1.2$ eV) exhibits a circular distribution, showing that the fragment anisotropy drastically changes by the electronic excitation. Polar plots in Figs. 2(c) and 2(d) compare the angular distributions of the $c^3\Pi$ component intensity for the two different initial states. Since the time scale of the dissociation is sufficiently shorter than typical rotational periods of NO (9 ps), the polar plots represent molecular-axis distributions after ionization. For the $X^2\Pi$ state, prominent peaks are seen about $\beta = 45°$ with respect to the polarization direction. On the other hand, the fragment from $A^2\Sigma^+$ formed a broad distribution centered at $\beta = 0°$, which is consistent with the Rydberg character of the $3s\sigma$ orbital [Fig. 1(a)].

In order to quantitatively evaluate the difference associated with the initial HOMOs, we carried out theoretical calculations using WFAT [21,22], which naturally include the effect of the permanent dipole of a heteronuclear diatomic molecule. The tunneling ionization rate in a static electric field F is expressed as

$$\Gamma(\beta, F) = \left[|G_{00}(\beta)|^2 + \frac{F}{2\varkappa^2} |G_{01}(\beta)|^2 \right] W_{00}(F), \quad (1)$$

where $G_{00}(\beta)$ and $G_{01}(\beta)$ are the orientation-dependent structure factors with β being the angle between the electric field and the molecular axis [see Fig. 1(b)], $\varkappa = \sqrt{2I_p}$ with I_p being the ionization potential, and

$$W_{00}(F) = \frac{\varkappa}{2} \left(\frac{4\varkappa^2}{F} \right)^{2/\varkappa - 1} \exp\left(-\frac{2\varkappa^3}{3F} \right) \quad (2)$$

is the field factor. The structure factors were calculated from a HOMO obtained within the Hartree-Fock approximation using the X2DHF [32,33] code. We took the values from the table in Ref. [34] for the ground state and newly calculated for the excited state. The ionization yields at a fixed β were then calculated by the integration over the 8 fs laser pulse with the peak intensity of 1.1×10^{14} W/cm^2 under the adiabatic approximation [35]. The results, plotted in Figs. 2(c) and 2(d), show excellent agreement with the experimental results for both the ground and excited states.

Finally, we discuss the validity of the tunneling ionization picture for the electronically excited state. Since the effective ionization potential from the excited state is only $I_p = 3.8$ eV (see Fig. 1), multiphoton processes could contribute to the observed fragment anisotropy. To clarify the ionization mechanism responsible for the results in Fig. 2, we studied the dependence of the fragment yields on the ellipticity of the probe laser polarization. Figure 4 plots the $c^3\Pi$ component yields against the angle θ of a quarter-wave plate inserted in the beam path of the probe pulse. The $c^3\Pi$ component yields are largest at $\theta = 0°$ (linear polarization) and steeply decrease to near zero values at $\theta = 45°$ (circular) for both initial states ($X^2\Pi$ and $A^2\Sigma^+$).

The observed ellipticity dependence is interpreted as follows. In linearly polarized light, the freed electron travels along the laser polarization direction to be rescattered by the ion core. The corresponding electron wave packet exhibits a transversal spread by the time of rescattering because of the initial momentum at the ionization. In elliptically polarized light, the electron trajectory is shifted laterally by the perpendicular component of the electric field. Since the lateral shift results in the decrease in the electron flux at the ion core, the fragment yields decrease as the increase in the ellipticity [28]. The probability density of the returning electron at the ion core ($r = 0$) can be expressed by using the adiabatic theory [35],

$$|\psi_0(t_i,\beta)|^2 \propto \frac{\Gamma(\beta,F(t_i))}{F(t_i)}\exp\left[-\frac{\varkappa \mathbf{u}_i^2(t_f,t_i)\Delta t^2/F(t_i)}{\varkappa^2/F^2(t_i)+\Delta t^2}\right], \quad (3)$$

where $\mathbf{u}_i(t_f,t_i)$ is the initial transversal velocity and $\Delta t = t_f - t_i$ with t_i and t_f being the ionization and rescattering time, respectively. This indicates that a smaller ionization potential (or $\varkappa$) provides a broader transversal distribution when $|\varkappa/F| \ll |\Delta t|$, which is consistent with the experimental results in Fig. 4 showing a broader distribution for the excited state than that for the ground state ($I_p = 9.26$ eV).

For a more quantitative discussion, the electric field of elliptically polarized light (angular frequency ω) is expressed as $\mathbf{F}(t) = \bar{F}(\sin\theta\sin\omega t\,\mathbf{e}_x + \cos\theta\cos\omega t\,\mathbf{e}_z)$, where we assume a constant amplitude $\bar{F}$ for simplicity. The rescattering condition $\mathbf{F}(t_i)\mathbf{u}_i(t_f,t_i) = 0$ [35] determines the relation between t_i and t_f as

$$\sin^2\theta[\omega\Delta t\cos\omega t_i - (\sin\omega t_f - \sin\omega t_i)]\sin\omega t_i$$
$$= \cos^2\theta[\omega\Delta t\sin\omega t_i + (\cos\omega t_f - \cos\omega t_i)]\cos\omega t_i, \quad (4)$$

which gives rise to

$$\mathbf{u}_i^2(t_f,t_i) = \frac{\bar{F}^2}{\omega^4\Delta t^2}(\omega\Delta t - \sin\omega\Delta t)$$
$$\times\left(\omega\Delta t - \frac{\sin\omega t_f - \sin\omega t_i}{\cos\omega t_i}\right)\sin^2\theta. \quad (5)$$

To calculate the electron rescattering excitation probability, a step function $\Theta(E - E_{th})$ at the excitation threshold energy $E_{th} = 12.5$ eV is assumed for the electron-impact excitation cross section from the ionic ground state to the $c^3\Pi$ state. The recolliding electron energy is expressed as $E(t_i) = |\mathbf{u}_f(t_f,t_i)|^2/2$ in terms of the momentum at the rescattering time $\mathbf{u}_f(t_f,t_i) = \mathbf{u}_i(t_f,t_i) - \int_{t_i}^{t_f}\mathbf{F}(t)dt$, where the second term is the velocity gained in the laser field. Finally, one can obtain the electron rescattering excitation probability by averaging over t_i for one optical cycle, and then by averaging over β for the molecular orientation as

$$P_{exc}(\theta) \propto \int_0^\pi \sin\beta d\beta \int_0^{2\pi/\omega} dt_i|\psi_0(t_i,\beta)|^2\Theta(E(t_i) - E_{th}),$$

$$(6)$$

where $|\psi_0(t_i,\beta)|^2$ is dependent on θ and set to zero for nonrescattering trajectories.

The resultant electron rescattering excitation probability $P_{exc}(\theta)$ was used for the least-squares fitting to the experimental data for the $X^2\Pi$ state, where $\bar{F}$ is treated as a fitting parameter. The obtained value $\bar{F} = 0.059(3)$ a.u. is in good agreement with the value ($F = 0.057$ a.u.) calculated from the estimated field intensity (1.1×10^{14} W/cm^2), thus confirming the rescattering mechanism for DI from the ground state. The dashed line in Fig. 4 shows $P_{exc}(\theta)$ calculated for the $A^2\Sigma^+$ state using the $\bar{F}$ value and the ionization potential $I_p = 3.8$ eV. The theoretical result agrees well with the experimental data, showing that DI from the excited state is dominated by the rescattering process of electrons produced by the tunneling ionization. Thus, the observed ellipticity dependence in Fig. 4 supports that the tunneling ionization and the electron rescattering are responsible for the dissociative ionization in both cases. Since the ground state of NO$^+$ is singlet ($X^1\Sigma^+$), the excitation to the dissociative triplet state ($c^3\Pi$) favors electron impact rather than multiphoton absorption, which explains the dominance of the tunneling and rescattering process in the present study.

In summary, we investigated the dissociative ionization of NO, NO $\rightarrow$ NO$^+$ + e^- $\rightarrow$ N$^+$ + O + e^-, in few-cycle intense laser fields (8 fs, 1.1×10^{14} W/cm^2), with two different initial states, $X^2\Pi$ and $A^2\Sigma^+$. Supported by quantitative comparisons with a solid theory on tunneling ionization and electron rescattering, the present study demonstrates a secure readout of the electron distribution in an excited molecule (and the change in the distribution by photoexcitation) by tunneling-ionization imaging with few-cycle intense laser pulses. The present study provides a deeper understanding of laser tunneling ionization of

molecules, a key step of important applications such as high-order harmonics generation and self-electron diffraction, and paves the way for real-time visualization of electron dynamics in chemical reactions.

---

*hishi@chem.nagoya-u.ac.jp

[1] G. R. Wu, P. Hockett, and A. Stolow, Phys. Chem. Chem. Phys. **13**, 18447 (2011).

[2] P. M. Kraus and H. J. Wörner, Chem. Phys. **414**, 32 (2013).

[3] F. Lépine, M. Y. Ivanov, and M. J. J. Vrakking, Nat. Photonics **8**, 195 (2014).

[4] F. Calegari, D. Ayuso, A. Trabattoni, L. Belshaw, S. De Camillis, S. Anumula, F. Frassetto, L. Poletto, A. Palacios, P. Decleva, J. B. Greenwood, F. Martin, and M. Nisoli, Science **346**, 336 (2014).

[5] P. Hockett, C. Z. Bisgaard, O. J. Clarkin, and A. Stolow, Nat. Phys. **7**, 612 (2011).

[6] A. Staudte, S. Patchkovskii, D. Pavicic, H. Akagi, O. Smirnova, D. Zeidler, M. Meckel, D. M. Villeneuve, R. Dörner, M. Y. Ivanov, and P. B. Corkum, Phys. Rev. Lett. **102**, 033004 (2009).

[7] M. Yamazaki, K. Oishi, H. Nakazawa, C. Zhu, and M. Takahashi, Phys. Rev. Lett. **114**, 103005 (2015).

[8] J. Itatani, J. Levesque, D. Zeidler, H. Niikura, H. Pepin, J. C. Kieffer, P. B. Corkum, and D. M. Villeneuve, Nature (London) **432**, 867 (2004).

[9] W. Li, X. Zhou, R. Lock, S. Patchkovskii, A. Stolow, H. C. Kapteyn, and M. M. Murnane, Science **322**, 1207 (2008).

[10] H. J. Wörner, J. B. Bertrand, D. V. Kartashov, P. B. Corkum, and D. M. Villeneuve, Nature (London) **466**, 604 (2010).

[11] X. M. Tong, Z. X. Zhao, and C. D. Lin, Phys. Rev. A **66**, 033402 (2002).

[12] J. Muth-Böhm, A. Becker, and F. H. M. Faisal, Phys. Rev. Lett. **85**, 2280 (2000).

[13] D. Pavičić, K. F. Lee, D. M. Rayner, P. B. Corkum, and D. M. Villeneuve, Phys. Rev. Lett. **98**, 243001 (2007).

[14] D. Dimitrovski, M. Abu-samha, L. B. Madsen, F. Filsinger, G. Meijer, J. Küpper, L. Holmegaard, L. Kalhøj, J. H. Nielsen, and H. Stapelfeldt, Phys. Rev. A **83**, 023405 (2011).

[15] A. Staudte, S. Patchkovskii, D. Pavicic, H. Akagi, O. Smirnova, D. Zeidler, M. Meckel, D. M. Villeneuve, R. Dörner, M. Y. Ivanov, and P. B. Corkum, Phys. Rev. Lett. **102**, 033004 (2009).

[16] J. Wu, L. P. H. Schmidt, M. Kunitski, M. Meckel, S. Voss, H. Sann, H. Kim, T. Jahnke, A. Czasch, and R. Dörner, Phys. Rev. Lett. **108**, 183001 (2012).

[17] A. S. Alnaser, S. Voss, X. M. Tong, C. M. Maharjan, P. Ranitovic, B. Ulrich, T. Osipov, B. Shan, Z. Chang, and C. L. Cocke, Phys. Rev. Lett. **93**, 113003 (2004).

[18] F. R. Gilmore, J. Quant. Spectrosc. Radiat. Transfer **5**, 369 (1965).

[19] D. L. Albritton, A. L. Schmeltekopf, and R. N. Zare, J. Chem. Phys. **71**, 3271 (1979).

[20] H. Partridge, S. R. Langhoff, and C. W. Bauschlicher, Jr., J. Chem. Phys. **93**, 7179 (1990).

[21] O. I. Tolstikhin, T. Morishita, and L. B. Madsen, Phys. Rev. A **84**, 053423 (2011).

[22] L. B. Madsen, O. I. Tolstikhin, and T. Morishita, Phys. Rev. A **85**, 053404 (2012).

[23] J. Luque and D. R. Crosley, J. Chem. Phys. **111**, 7405 (1999).

[24] A. Hishikawa, E. J. Takahashi, and A. Matsuda, Phys. Rev. Lett. **97**, 243002 (2006).

[25] H. Hasegawa, A. Hishikawa, and K. Yamanouchi, Chem. Phys. Lett. **349**, 57 (2001).

[26] N. B. Delone and V. P. Krainov, J. Opt. Soc. Am. B **8**, 1207 (1991).

[27] A. Lafosse, M. Lebech, J. C. Brenot, P. M. Guyon, O. Jagutzki, L. Spielberger, M. Vervloet, J. C. Houver, and D. Dowek, Phys. Rev. Lett. **84**, 5987 (2000).

[28] H. Niikura, F. Légaré, R. Hasbani, A. D. Bandrauk, M. Y. Ivanov, D. M. Villeneuve, and P. B. Corkum, Nature (London) **417**, 917 (2002).

[29] M. F. Kling, C. Siedschlag, A. J. Verhoef, J. I. Khan, M. Schultze, T. Uphues, Y. Ni, M. Uiberacker, M. Drescher, F. Krausz, and M. J. J. Vrakking, Science **312**, 246 (2006).

[30] I. Bocharova, R. Karimi, E. F. Penka, J.-P. Brichta, P. Lassonde, X. Fu, J.-C. Kieffer, A. D. Bandrauk, I. Litvinyuk, J. Sanderson, and F. Légaré, Phys. Rev. Lett. **107**, 063201 (2011).

[31] G. Herzberg, *Spectra of Diatomic Molecules*, 2nd ed. (Van Nostrand, New York, 1950).

[32] J. Kobus, L. Laaksonen, and D. Sundholm, Comput. Phys. Commun. **98**, 346 (1996).

[33] http://www.leiflaaksonen.eu/num2d.html.

[34] R. Saito, O. I. Tolstikhin, L. B. Madsen, and T. Morishita, At. Data Nucl. Data Tables **103–104**, 4 (2015).

[35] O. I. Tolstikhin and T. Morishita, Phys. Rev. A **86**, 043417 (2012).